# New High-Resolution Solution for Measuring Degree of Sensitization of Duplex Stainless Steel 2205 Using Double-Loop Electrochemical Potentiodynamic Reactivation Technique

*B. Hashemi,* A. Davoodi,** M. Momeni,‡,* and M.H. Moayed**

## ABSTRACT

*In the present work, a new high-resolution solution for measuring degree of sensitization (DOS) of duplex stainless steel (DSS) 2205 (UNS S31803) by double loop-electrochemical potentiodynamic reactivation (DL-EPR) technique was obtained and the solution parameters were optimizing using the Taguchi method. Sensitized samples in three different conditions were chosen and five solution main factors including acid and two types of depassivator concentrations, scan rate, and surface roughness were considered. To reduce the number of experiments, Taguchi orthogonal array (OA) was used. The resulting optimal condition was to be 0.5 M sulfuric acid ($H_2SO_4$), 0.002 M sodium thiosulfate ($Na_2S_2O_3$), 0.02 M sodium chloride (NaCl), and 120 grid in surface roughness and 30 mV/min scan rate. By introducing the new solution, a DOS value of 78% was obtained in the DSS2205 sample sensitized at 850°C for 40 min. Moreover, topography variations of non-sensitized and sensitized samples measured by atomic force microscopy elucidated the mechanism of austenite/ferrite boundary attack and carbide precipitates formation in sensitized samples extended to the ferrite phase.*

*KEY WORDS: atomic force microscopy, double-loop electrochemical potentiodynamic technique, duplex stainless steel, sensitization, Taguchi method*

## INTRODUCTION

Duplex stainless steels (DSS) composed of duplex phases of austenite and ferrite are used extensively in the oil, gas, and chemical industries because of their higher mechanical strength and excellent resistance to pitting corrosion, stress corrosion cracking (SCC), and intergranular corrosion (IGC). Generally, these alloys have higher tensile strength and exhibit greater resistance to localized corrosion than Type 300-series austenitic stainless steels.[1] The superior properties of these alloys are primarily a result of the presence of approximately equivalent amounts of austenite and ferrite in the microstructure.[2] Chromium is responsible for the corrosion resistance because it permits the formation of the passive layer on the steel surface, a dense and closed protective film based on chromium oxide. Owing to this potential-dependent passivation, the steel remains passive in contact with many aggressive media.[3] However, precipitation of detrimental phases, such as chromium carbides ($Cr_{23}C_6$ or $M_7C_3$), nitrides ($Cr_2N$), and intermetallic phases (sigma, chi, etc), inevitably occur when DSS is heated to temperatures ranging from 300°C to 1,000°C during manufacturing, heat treating, or welding. These precipitates will lead to the reduction of corrosion resistance of DSS as a result of the presence of Cr-depleted zones around these precipitates and cause IGC.[4-8] The increasing demands on safety inevitably lead to the need for testing methods, which can detect the susceptibility to corrosion accurately and with a minimum of time need.[9]

Submitted for publication: March 29, 2012. Revised and accepted: July 26, 2012. Preprint available online: October 17, 2012, http://dx.doi.org/10.5006/0699.

‡ Corresponding author. E-mail: mojtaba.momeni@stu.um.ac.ir.
* Metallurgical and Materials Engineering Department, Ferdowsi University of Mashhad, Mashhad 91775-1111, Iran.
** Materials Engineering Department, Hakim Sabzevari University, Sabzevar 391, Iran.


ISSN 0010-9312 (print), 1938-159X (online)
13/000043/$5.00+$0.50/0  

There are a number of standard methods, such as the oxalic acid test, Strauss test, Huey test, Streicher test, and copper-copper sulfate-50% sulfuric acid test, which can be used to assess the susceptibility to IGC. None of these methods are a quantitative and non-destructive method. Moreover, performing the above-mentioned tests is time-consuming. During the past decades, much research has been conducted to innovate a test method by developing the electrochemical potentiodynamic reactivation (EPR) test. The EPR is a quantitative method that indicates degree of sensitization (DOS) based on electrochemical parameters obtained from the potentiodynamic polarization curve.[10-16]

The EPR test performed in 2.5 M sulfuric acid ($H_2SO_4$) solution was first introduced in 1969 by Cihal, et al.,[17] and then in 1977, Clarke, et al.,[18] proposed a single-loop EPR method executed in 0.5 M $H_2SO_4$ + 0.01 M potassium thiocyanate (KSCN) solution, which required very fine surface polish (1 μm) and time-consuming measurement of grain size. Finally, Akashi, et al.,[19] developed a double-loop EPR (DL-EPR) method in 1980, and the advantage of this method lies in its independence of both the inclusion contents of the material and its surface finish.

It also must be borne in mind that all these EPR tests were designed originally for 300 series austenite stainless steels,[20-21] and the first work for investigating the IGC susceptibility of a DSS was not reported until 1986 by Scully and Kelly.[22]

With the increased use of DSS, a few literatures had focused on the application of the modified DL-EPR to DSS, and the main applied electrolyte were $H_2SO_4$ solution with the addition of sodium chloride (NaCl), KSCN or thioacetamide ($CH_3CSNH_2$) as depassivators.[23-29] Hydrochloric acid (HCl) was first used for super austenite stainless steel DOS measurement in 1997 and then extended to 22% and 25% in Cr DSS since 2001.[30-33]

The detailed description of the single-loop (SL)-EPR and the DL-EPR can be found in the literature.[15-16] Here, in brief, it can be highlighted that the results of the DL-EPR are reported as a ratio of current density and/or the charge consumed during the reactivation scanning stage to the current and/or the charge created during the activation scanning stage:

$$\text{DOS}\% = \frac{i_r}{i_a} \times 100 \text{ or } \text{DOS}\% = \frac{Q_r}{Q_a} \times 100 \qquad (1)$$

where $i_r$ is the maximum current density during the reactivation scan, $i_a$ is the overall current density during the activation scan, $Q_r$ is the overall anodic charge measured during the reactivation scan, and $Q_a$ is the maximum charge measured during the activation scan.[16]

Several factors can influence the resolution of the DOS measurement, including acid and depassivator concentration, temperature, scan rate, reverse potential, etc. This indicates that DOS is a multi-variant parameter and investigating the effect of individual factors is essential.[34] Since DOS includes a significant number of factors, a full factorial design of the experiments requires a large number of runs and measurements, which are all time-consuming and costly. One of the well-known statistical methods to reduce the number of tests with comparable accuracy is the Taguchi method. Taguchi method is a design of experiment base approach to reduce the number of experiments and evaluate the effects of various parameters and their interactions on the required characteristic and obtain the optimum condition of the effective parameters.[35-36]

In the present study, the Taguchi method was used to determine the influence of the main factors on the DOS measuring resolution of DSS2205, and a new solution for DOS determination of this alloy is introduced. Moreover, topography variations of non-sensitized and sensitized samples, austenite/ferrite boundary attack morphology, and carbide precipitates formation in sensitized sample were studied using atomic force microscopy (AFM).

## EXPERIMENTAL PROCEDURES

### *Material and Heat Treatments*

The chemical composition analysis of the alloy in weight percent was 0.03% C, 0.97% Mn, 0.022% P, 0.0007% S, 0.74% Si, 21.61% Cr, 5.31% Ni, 3.07% Mo, 0.16% Cu, 0.136% V, 0.064% W, 0.01% Ti, 0.15% N, and Fe balance, which is in agreement with the AISI 2205 (UNS S31803). The alloy was annealed at 1,060°C for 40 min and quenched in water to dissolve any probable formed precipitation during the production process. After that, two specimens were subjected to sensitization, one at 650°C and other at 850°C for 40 min. The peak is 850°C of the time-temperature-transformation (TTT) diagram of sensitization of DSS2205, and sensitization at this temperature produces a complete sensitized specimen. The other specimen (sensitized at 650°C) is sensitized slightly since at this temperature no considerable precipitate can form. Both specimens after sensitization were quenched in water. The microstructure of specimens was characterized using optical microscopy. For this purpose, the specimens were mechanically grinded down to 1,200 silicon carbide (SiC) grit and then polished to 0.05 μm by alumina slurry. The specimens were electrically etched in 10% oxalic acid ($H_2C_2O_4$) solution by passing current of 1 A/cm$^2$ according to the ASTM A262, practice A.[37] Since this standard was not developed for DSS, the microstructure cannot be categorized based on this standard; however, it is helpful for determining the depleted zones because they are dissolved by this etching process.

**TABLE 1**
*Defined Factors and Their Levels*

| Factor | Level | | | |
|---|---|---|---|---|
| | 1 | 2 | 3 | 4 |
| $H_2SO_4$ concentration (M) | 0.5 | 0.8 | 1.0 | 1.5 |
| $Na_2S_2O_3$ concentration (M) | 0.002 | 0.003 | 0.004 | 0.005 |
| NaCl concentration (M) | 0 | 0.005 | 0.01 | 0.02 |
| Surface roughness | 120 | 600 | 1,200 | 1 µm |
| Scan rate (mV/min) | 30 | 60 | 90 | 120 |

## Taguchi Method

The Taguchi test design was used for DOS measuring of DSS2205. Five different parameters that influence the DOS results, including $H_2SO_4$ concentration, sodium thiosulfate ($Na_2S_2O_3$), and NaCl concentrations as two different depassivators, surface roughness and scan rate were chosen and from each factor four different levels were defined. The parameters and their levels were listed in Table 1. There are standard orthogonal arrays (OA), which suggest the number of tests and their conditions in the Taguchi method. In addition, the methodology of finding these arrays and producing non-standard arrays are described in detail in the Taguchi reference book.[36] Considering five factors and four levels from each, 1,024 experiments should be done. The Taguchi method introduces an $L'_{16}$ orthogonal array by which the number of experiment reduces to 16 with almost similar reliability on the results. These 16 experiments are listed in Table 2, and DOS of both sensitized specimens were measured in these conditions. The results of the Taguchi method can be reported as a signal to noise (S/N) ratio. Different strategies for S/N calculation were proposed.[35-36,38-39] Since, in this study, the goal was to achieve the highest resolution of DOS measurement, type B was chosen with the following formula:

$$S/N_B = -10 \times \log_{10}\left(\frac{1}{r}\sum\frac{1}{y_i^2}\right) \quad (2)$$

where $y_i$ is the desired property, which is DOS in this case, and r is the number of repetitions of each experiment.

The purpose of the analysis of variance (ANOVA) is to investigate which parameters of process significantly affect DOS value. Details of ANOVA can be seen elsewhere,[34-35] but, in brief, the analysis can be accomplished by separating the total variability of the S/N ratios, which is measured by the sum of the squared deviations (SS) from the total mean of the S/N ratio, ($S_m$), into contributions by each process parameter. Equations for calculating the variance of DOS measurement are:[34-35,39]

$$S_m = \frac{\left(\sum_{i=1}^{N} S/N_i\right)^2}{n} \quad (3)$$

where $S_m$ is correction factor and n is number of experiments in the matrix, which is 16 in this research.

$$SS_i = \frac{\sum_{j=1}^{L}\left(\frac{n}{L}m_{ij}\right)^2}{\frac{n}{L}} - S_m \quad (4)$$

$SS_i$ is the sum of square of factor i; $m_{ij}$ is the average of S/N ratio of factor i in level j, and L is the number of level for each factor, which is 4 in this research.

$$S_T = \sum_{i=1}^{N}(S/N_i)^2 - S_m \quad (5)$$

$S_T$ is total sum of square.

**TABLE 2**
*$L'_{16}$ Orthogonal Array*

| Experiment No. | Factor | | | | |
|---|---|---|---|---|---|
| | Acid Concentration | Thiosulfate Concentration | NaCl Concentration | Surface Roughness | Scan Rate |
| 1 | 1 | 1 | 1 | 1 | 1 |
| 2 | 1 | 2 | 2 | 2 | 2 |
| 3 | 1 | 3 | 3 | 3 | 3 |
| 4 | 1 | 4 | 4 | 4 | 4 |
| 5 | 2 | 1 | 2 | 3 | 4 |
| 6 | 2 | 2 | 1 | 4 | 3 |
| 7 | 2 | 3 | 4 | 1 | 2 |
| 8 | 2 | 4 | 3 | 2 | 1 |
| 9 | 3 | 1 | 3 | 4 | 2 |
| 10 | 3 | 2 | 4 | 3 | 1 |
| 11 | 3 | 3 | 1 | 2 | 4 |
| 12 | 3 | 4 | 2 | 1 | 3 |
| 13 | 4 | 1 | 4 | 2 | 3 |
| 14 | 4 | 2 | 3 | 1 | 4 |
| 15 | 4 | 3 | 2 | 4 | 1 |
| 16 | 4 | 4 | 1 | 3 | 2 |

$$MS_i = \frac{SS_i}{DF_i} \quad (6)$$

$MS_i$ is the mean sum of the square of factor i, where $DF_i$ is the degree of freedom of factor i, and that is the number of levels minus 1.

$$\rho(\%) = \frac{SS_i}{S_T} \times 100 \quad (7)$$

where ρ(%) is the percentage contribution for factor i.

### *Electrochemical Methods*

A conventional three-electrode cell was used for measuring DOS of sensitized specimens. In this cell, the mentioned specimens, i.e., sensitized and annealed, which were mounted in self-cure acrylic, were used as working electrodes, and a saturated calomel electrode (SCE) and platinum wire were used as reference and auxiliary electrodes, respectively. An automated potentiostat was used for electrochemical testing.

The DL-EPR were carried out in different conditions, as summarized in Table 2, and in 2.0 M $H_2SO_4$ + 0.01 M KSCN + 0.5 M NaCl, with 100 mV/min scan rate as a one of proposed procedures for determining DOS of DSS alloys.[40]

For measuring DOS by these experiments, the DL-EPR method was used in which the specimens were polarized from 50 mV below corrosion potential to anodic potentials in the passive state ca. 100 mV in conditions mentioned in Table 2. All measurements were carried out at ambient temperature. Before each experiment, the working electrode remains in solution for at least 15 min to reach the steady state. The experiments were repeated to ensure reproducibility.

### *Sample Preparation for Atomic Force Microscopy*

AFM observations were performed selectively on two samples, nonsensitized and sensitized samples at 850°C. The goal was to differentiate between their structures. For sample preparation, samples were abraded mechanically with SiC paper up to 2400 mesh and then were polished with 1 μm polycrystalline diamond paste, cleaned in ethanol ($CH_3CH_2OH$), and finally polished with a 0.25 μm polycrystalline diamond paste. After cleaning in ethanol, samples were slightly etched electrically in 10% oxalic acid solution with 0.5 A/cm$^2$ current density. The samples were dried and transferred immediately to the AFM characterization by a commerical instrument in contact mode operation.

## RESULTS AND DISCUSSION

### *Microstructure Analysis*

Figure 1 shows the microstructure of DSS2205 alloy, annealed and sensitized for 40 min at 650°C and 850°C. Darker phases represent ferrite and brighter phases are austenite. The annealed specimen did not show any dissolved precipitates at grain boundaries. In other words, in this specimen, no grain boundary precipitation can be found and there are only steps at boundaries. The sensitized specimens at 650°C and 850°C show dissolved precipitates at grain

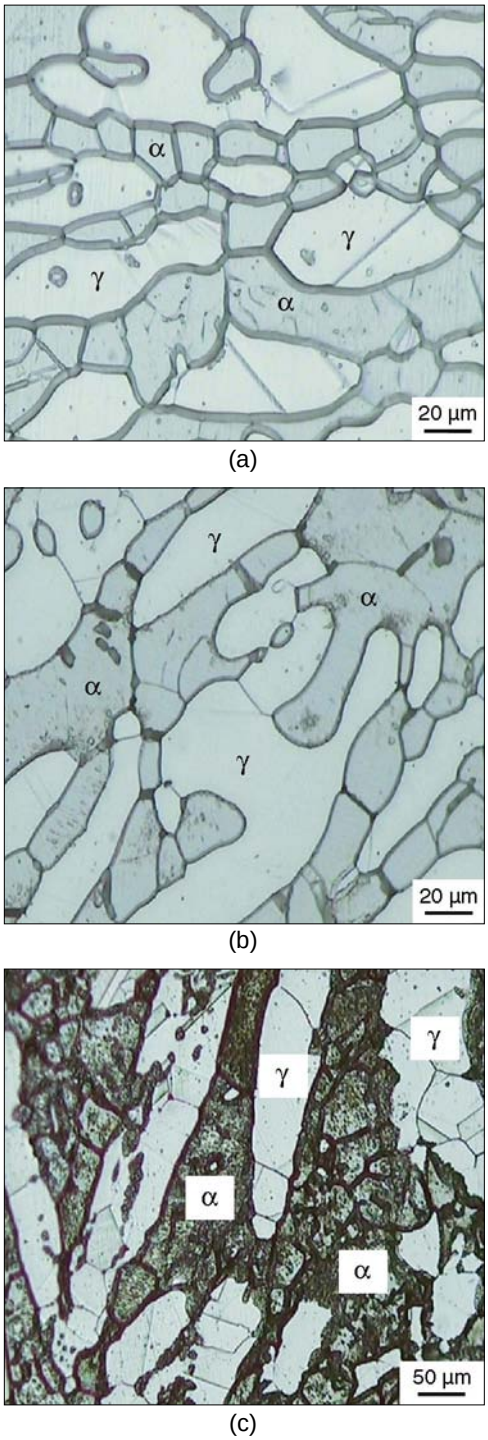


**FIGURE 1.** *Microstructure of DSS2205 alloy: (a) annealed, (b) sensitized for 40 min at 650°C, and (c) sensitized for 40 min at 850°C samples.*

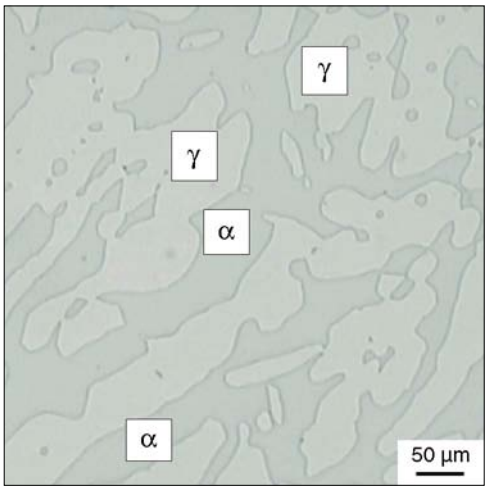


**FIGURE 2.** *Microstructure of nonsensitized sample prepared for AFM investigations using an optical microscope.*

boundaries. It is obvious that the amount of dissolved precipitates in the higher temperature, sensitized sample is significantly higher than those of 650°C. However, both samples show sensitization and, because of the intermetallic phase formation, depleted zones are formed in them. As a result of aging of the specimen at 850°C, some precipitates are formed at grain boundaries that dissolved in the etching process. Since 850°C is the critical temperature in the TTT diagram of precipitation of the DSS2205 alloy,[41] many types of precipitates can be formed in this temperature. It is reported that after aging of DSS2205 at 850°C, sigma phases are formed in boundaries of ferrite and austenite, and the volume fraction of chi phase in compression with sigma phase is negligible.[41] It is also reported that in this temperature $Cr_2N$ precipitates could be found in boundaries of ferrite and austenite, and ferrite/ferrite boundaries by increase in time. However, the main type of precipitation of both temperatures is sigma phase as it reported previously.[42]

By looking to the microstructure of these specimens, it is obvious that the precipitate growth direction is in ferrite phase. In other words, the precipitates are more likely to grow into ferrite rather than austenite. This can be attributed to the fact that, since chromium and molybdenum content of ferrite is higher than austenite and the diffusion coefficient of chromium in ferrite is almost 100 times higher than austenite,[41] the precipitates like chromium carbides, sigma phase, chi, etc., grow into the ferrite phase. On the other hand, higher value and diffusion coefficient of these elements in ferrite led to two different chromium- (and molybdenum-) depleted profiles in austenite and ferrite grains. The profile in austenite is narrow and deep and in ferrite is wide and shallow.[43] As a result, as it can be seen in the microstructure of these specimens, it seems that the precipitates were formed in ferrite phase.

### *Atomic Force Microscopy Results*

Figure 2 shows the optical microscopic image of microstructure of the nonsensitized sample that was prepared for AFM investigations. As it is mentioned in the "Microstructure Analysis" section, two phases are seen that include ferrite (darker regions) and austenite (brighter regions). Figure 3 shows 2D AFM images of the microstructure of a non-sensitized sample in different magnifications. In these images, the height variations between surface characteristics are shown. The microstructure contains ferrite, the darker phase, austenite, and the brighter phase (some brighter points are pollutions that have not been removed after ultrasonic cleaning). The ferrite is more corroded than austenite under etching conditions and there are no ditches in phase boundaries. This fact can be shown with more details in Figure 4, which shows two AFM images with some surface roughness profiles through phase boundaries. It can be seen that, in all phase boundaries, there are not any ditches by passing from austenite or ferrite to another. Figure 5 shows 3D AFM images related to the images in Figure 4.

Figure 6 shows the metallographic microstructure of the 850°C sensitized sample by an optical microscopic image. Although the etching process was light, it can be seen that phase boundaries are corroded because of their sensitization, and ferrite (darker regions) is corroded in some points. Two-dimensional AFM images of the 850°C sensitized sample in different magnifications are shown in Figure 7. The microstructure contains ferrite (darker region) and austenite (brighter regions) similar to the non-sensitized sample. However, in contrast, the phase boundaries in the 850°C sensitized sample shows quite dark bands with the lowest height. These are ditches at some parts of phase boundaries. This claim can be investigated more by profiles shown in Figures 8 and 9. In Figure 8(a), an AFM image of the 850°C sensitized sample (43.5 μm by 43.5 μm) with some vectors that pass from austenite-ferrite boundaries are shown. Also, the roughness profiles related to these lines are shown in Figure 8(b). It is obvious that lines 1, 2, and 3 and the related profiles depict the ditches in phase boundaries between austenite and ferrite at the points that are dark points in the boundaries. But the profile related to line 4, which crosses from ferrite to austenite and from austenite to ferrite in some other boundaries, does not illustrate any ditches in the boundaries, so it can be demonstrated that these boundaries are not sensitized. Also, Figure 9(a) shows another 2D AFM image (20 μm by 20 μm) of the surface of 850°C sensitized sample with three lines that pass from phase boundaries. Related profiles that depict surface roughness in the path of the lines in Figure 9(a) are shown in Figure 9(b). These profiles show that line 1 first passes from a boundary that has a ditch, but the second boundary in its path does not show any ditches, which indicates that this boundary is not

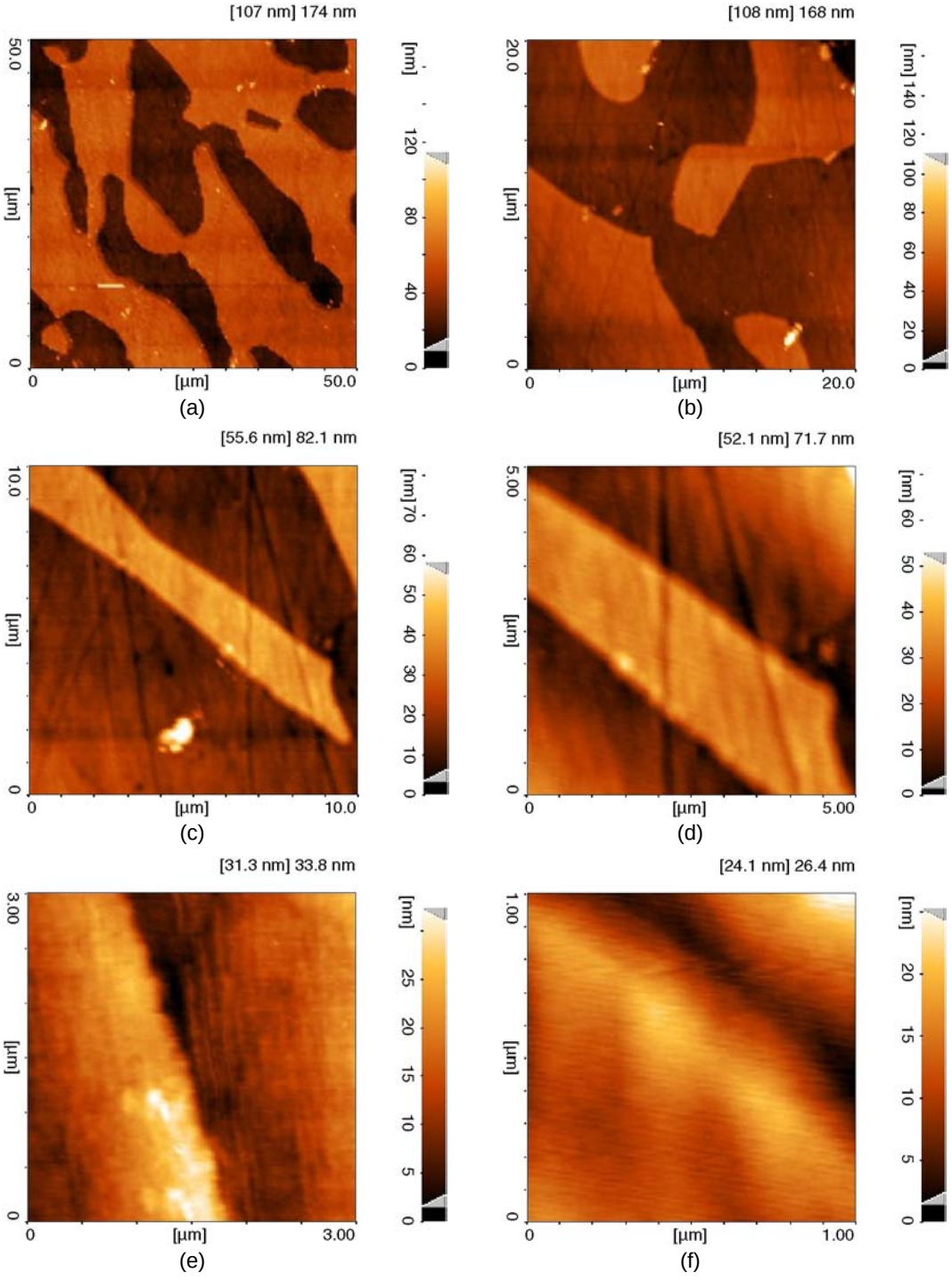


**FIGURE 3.** *Two-dimensional AFM images of nonsensitized sample: (a) through (f) different magnifications 50 µm by 50 µm to 1 µm by 1 µm, respectively.*

sensitized. Also, both boundaries and the boundary in the path of lines 2 and 3, respectively, show ditches.

So it can be concluded that the ditches are the sensitized boundaries that are caused from electro-etching in oxalic acid; they are corroded more than other surface characteristics. Also, there are some quantitative data that can be extracted from the profiles. These data are reported in Table 3. It contains the lateral expansion of the corrosion effect from the ditch's depth to the ferrite and austenite phases. It can be seen that, in all profiles, corrosion in ferrite is wider than that in austenite. As mentioned above, this phenomenon can be explained by the fact that in DSS, because the alloying elements like chromium and molybdenum are needed for formation, the passive layer in ferrite are more than that in austenite, so

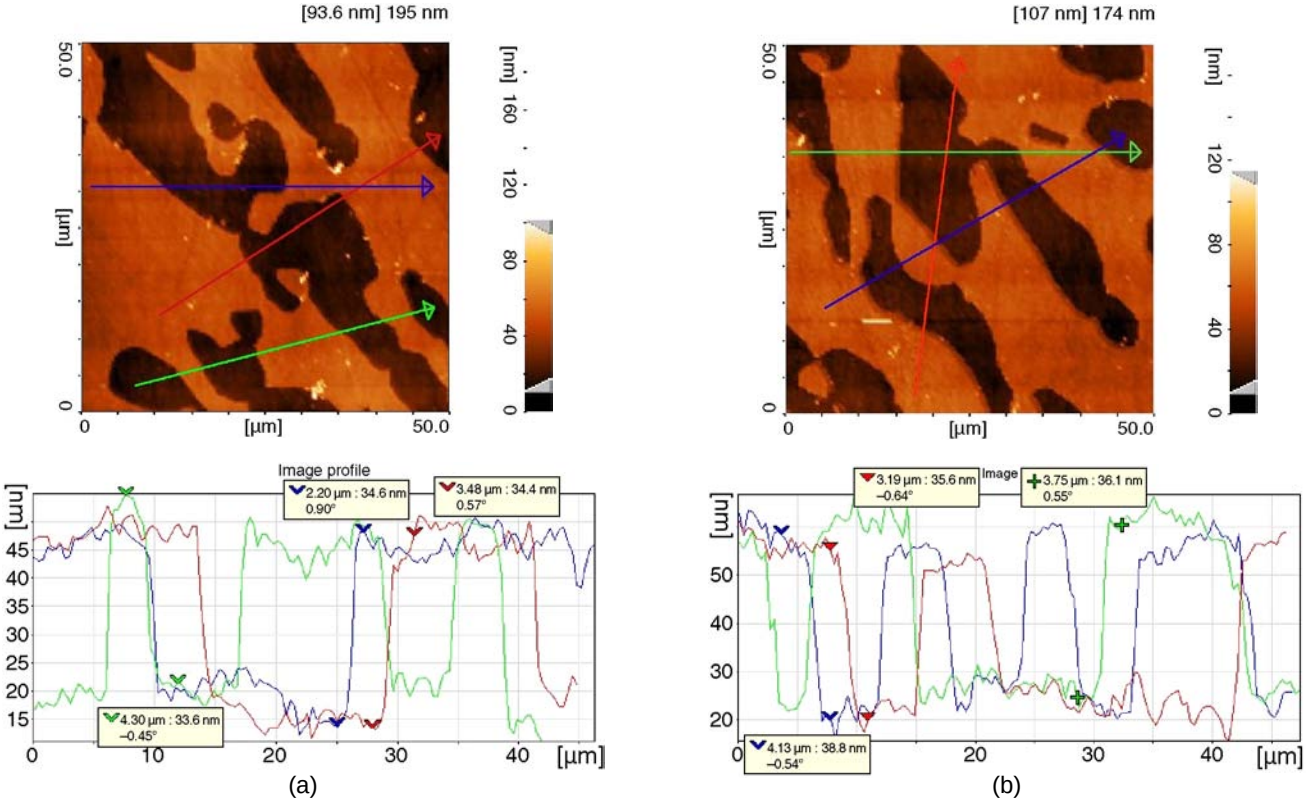


**FIGURE 4.** *Surface roughness profiles of the nonsensitized sample related to same color vectors in the AFM images.*

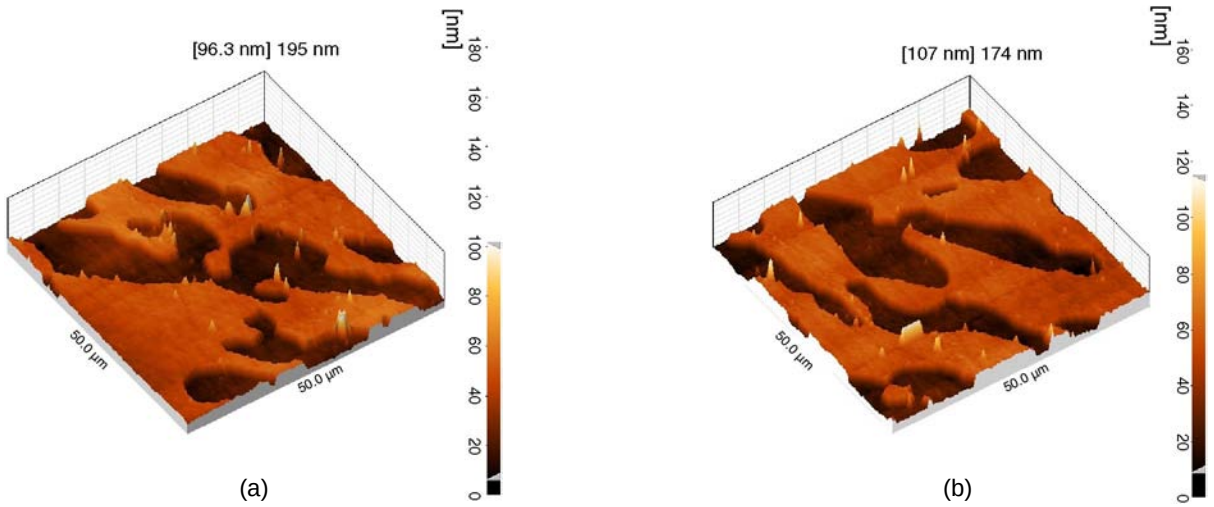


**FIGURE 5.** *Three-dimensional AFM images of nonsensitized sample related to the 2D AFM images in Figure 3.*

secondary phases in grain boundaries that need these elements to growth, like sigma phase, tend to growth in the ferrite rather than austenite. Figures 10(a) and (b) show AFM images that are the 3D form of Figures 8(a) and 9(a), respectively. The ditches are clear in these images and in Figures 10(c) and (d), by passing a lateral plane (blue plane), the differences between the height of ditches and ferrite and austenite phases are indicated.

Another remarkable point that should be declared is that, in all 2D and 3D AFM images of 850°C sensitized sample, no phase boundary is found that was fully sensitized, and all images indicated that some parts of the phase boundaries did not show any ditches and sensitization. However, optical microscope images for this specimen showed that all boundaries were sensitized as a result of the temperature of sensitization.

### *Taguchi Results*

Table 4 shows the DOS value and S/N ratios of both sensitized specimens calculated from Equation (2) (charge ratio) for each experiment. To compare the

influence of DOS parameters, the average S/N ratio for both specimens and each level is summarized and shown in Figure 11. Higher average S/N ratio for each level means greater effect of that level. Moreover, larger differences between average S/N ratios among all levels of a certain factor means that the factor has a higher effect on the DOS measurement. Average S/N ratios of each level for each factor are the mean value of the S/N ratio for all the experiments with the same level. For instance, for the surface roughness factor, the average S/N ratio for level 2 is the average of S/N ratios of experiments nos. 2, 8, 11, and 13. Regarding the above description, it can be seen that $H_2SO_4$ concentration has a significant influence on DOS measurement of both samples. By increasing $H_2SO_4$ concentration, the average S/N ratio increases, and as a result, resolution of DOS measurement increases consequently. This indicates that the most important factor in DOS measurement is acid concentration, since it gives a higher average S/N ratio in comparison with other factors. In addition, for both specimens, level 4 of acid concentration, i.e., 1.5 M $H_2SO_4$, has the highest average S/N ratio, which means in this concentration of acid, the highest DOS can be obtained for both specimens.

After acid concentration, scan rate and surface roughness have a higher influence on DOS resolution. However, in the case of the sample sensitized at 650°C, the influence of surface roughness is significant, and its influence is comparable w-ith that of acid concentration. On the other hand, for the 850°C sensitized specimen, the influence of scan rate is higher than that of surface roughness. This means that in the condition in which the alloy is slightly sensitized, e.g., 650°C, the surface condition has great influence on the corrosion resistance, and the rougher surface provided lower corrosion resistance and, consequently, a higher DOS value. However, when the specimen has been sensitized considerably, it is not significantly important what the surface roughness is. As it is previously reported,[21] surface roughness in the DL-EPR method is not important, unlike the SL-EPR, in which the surface must be polished down to 1 μm.[40] However, these results show that the surface roughness is an important task in DOS measurement when the specimen is slightly sensitized, and it is not important when considerable sensitization occurs during the sensitization process. However, for both specimens the rougher surface gives higher DOS, which was predictable. Effect of scan rate in the specimen, which is slightly sensitized, is much lower than surface roughness, and it is much higher than surface roughness for the 850°C sensitized specimen. In other words, at low sensitization conditions, after acid concentration, the surface roughness is very important, and in circumstances in which the alloy is completely sensitized, the scan rate of the DL-EPR test is very important. This is because the depleted area in high sensitized specimens is higher than low sensitized ones. As a consequence, a lower scan rate makes the condition more appropriate for passivity breakdown in grain boundary areas. However, the optimum level has not differed for highly or lowly sensitized specimens, and it is 30 mV/min.

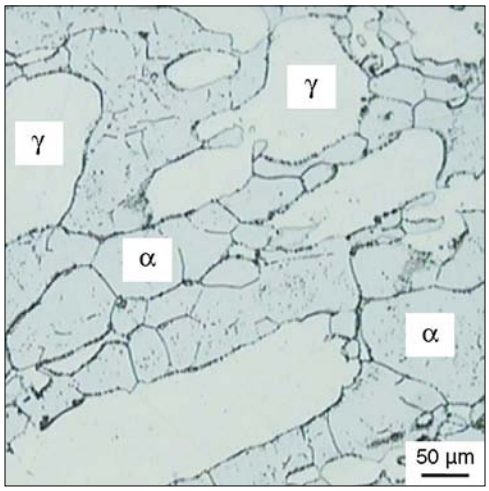


**FIGURE 6.** *Microstructure of 850°C sensitized sample prepared for AFM investigations by optical microscope.*

In this study, two types of depassivators were used simultaneously to investigate their effects on the DOS measurement. One of them is the thiosulfate ion in the form of sodium thiosulfate salt ($Na_2S_2O_3$), which is reported previously by authors as a depassivator agent in the DL-EPR method.[44] The other one is chloride ions in the form of NaCl salt that was previously introduced for the DOS measuring of DSS2205.[45] The results of both sensitized specimens show that the depassivating effect of the thiosulfate ion is higher than that of the chloride ion. The mechanism of depassivation of the thiosulfate ion is previously reported.[44] Here, in brief, the thiosulfate ion in acidic solutions and on the surface of metal reduced to adsorbed sulfur on the surface and the adsorbed sulfur itself reduced to $H_2S$. The $H_2S$ then breaks down the passivity of iron (in the depleted areas) and has no influence on the passivity of chromium (inside the grains). On the other hand, the effect of chloride ion on the passivity of stainless steels is well known and the passivity in presence of chloride is more deteriorated than its absence.[46-49] As a result, the presence of chloride ion may assist the passivity breakdown in the DL-EPR method. The results show that the average S/N ratio for different chloride ions is almost similar, indicating a low influence of the chloride ion on the results of the measured DOS. The effect of thiosulfate ion is higher than chloride; however, it is still lower than previously reported factors. As it can be seen, by increasing the chloride concentration, the average S/N ratio for both samples increases. This indicates that in the presence of a higher amount of

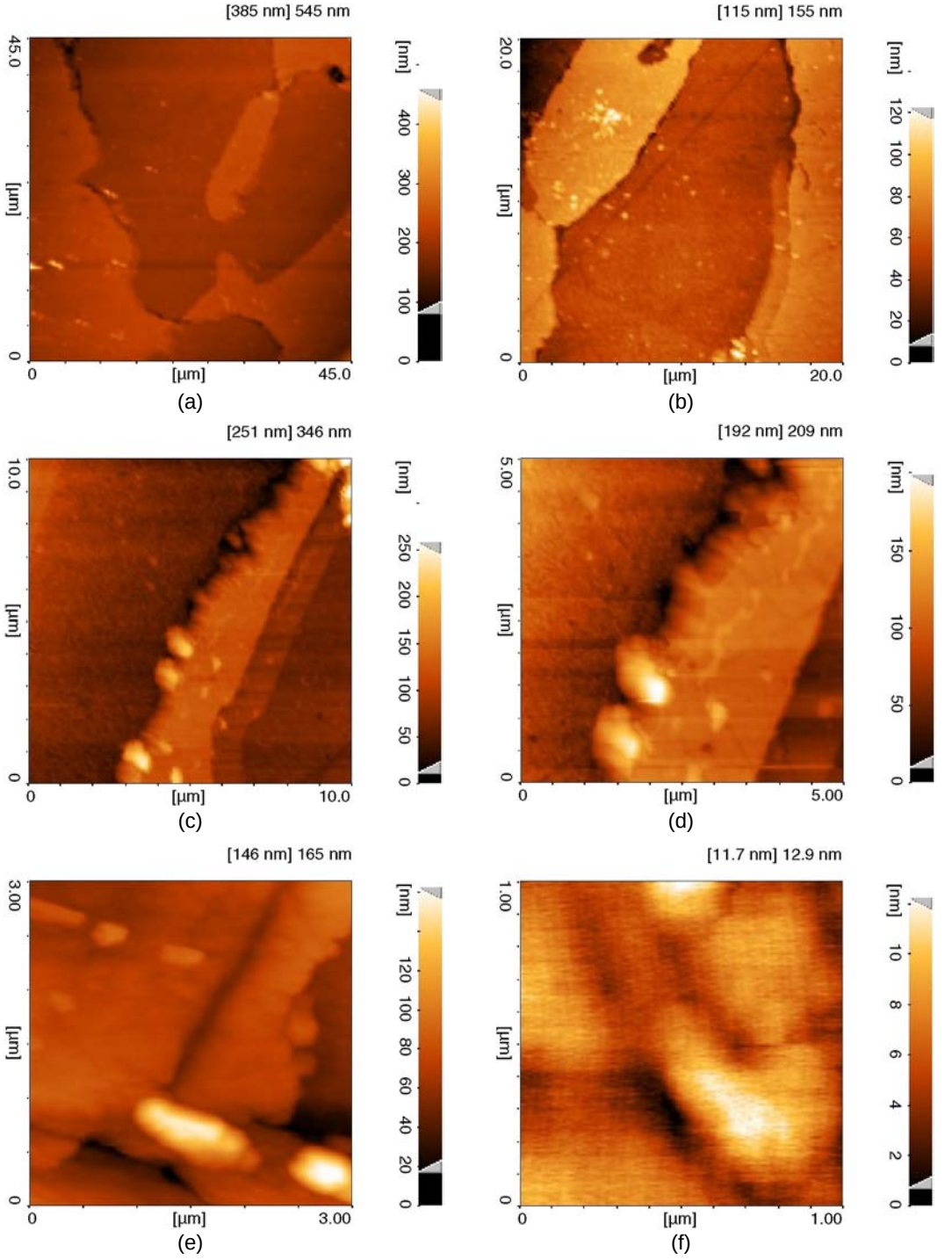


**FIGURE 7.** *Two-dimensional AFM images of 850°C sensitized sample: (a) through (f) different magnifications 45 µm by 45 µm to 1 µm by 1 µm, respectively.*

chloride ion, in the reactivation stage, passivity breakdown occurs more easily. In the case of thiosulfate ions, the lowest concentration gives the highest efficiency and the resolution decreases by increasing the thiosulfate concentration up to level 3, i.e., 0.004 M, and by a further increase in concentration, the resolution increases. The fact that increasing the thiosulfate concentration up to level 3 decreases the resolution is the cathodic reaction of reduction of thiosulfate to sulfur. This reaction was reported previously[44] and it was shown that the redox potential of this cathodic reaction is high enough to form adsorbed sulfur on the surface in the anodic potentials. Increasing the amount of thiosulfate ion increases the current density of this cathodic reaction and, hence, masks the anodic current density formed during the reactiva-

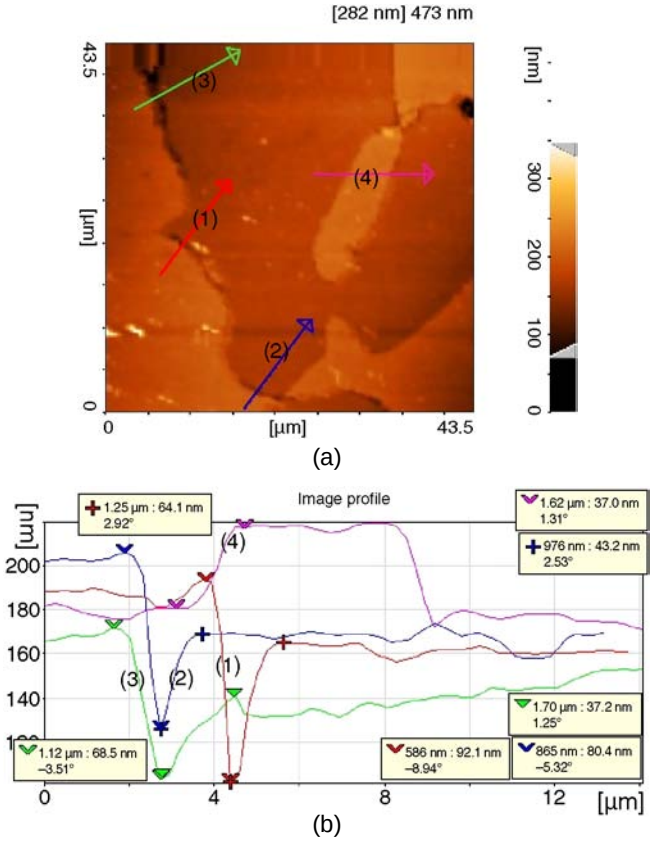


**FIGURE 8.** *(a) Two-dimensional AFM image of 850°C sensitized sample (43.5 µm by 43.5 µm) with vectors pass from phase boundaries and (b) profiles related to the vectors in the AFM image in (a).*

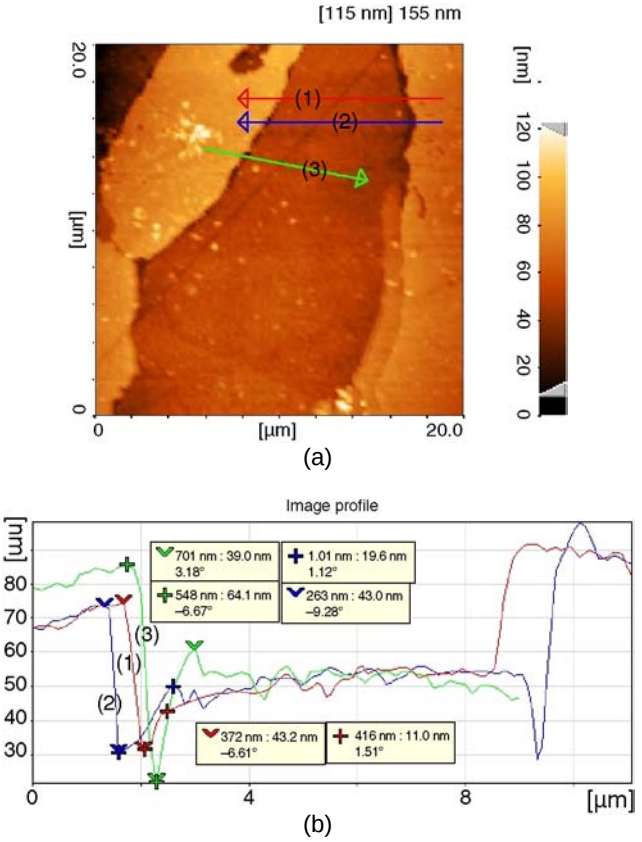


**FIGURE 9.** *(a) Two-dimensional AFM image of 850°C sensitized sample (20 µm by 20 µm) with vectors pass from phase boundaries and (b) profiles related to the vectors in the AFM image in (a).*

tion stage. With a further increase in its concentration to 0.005 M, the average S/N ratio increases, which means, as a result of the higher aggressivity of solution, DOS resolution increases. A quantitative analysis of the effect of each parameter on the DOS measurement will be discussed in the next section.

By looking to the Taguchi results, the new condition for both heat treatments is 1.5 M $H_2SO_4$ + 0.005 M $Na_2S_2O_3$ + 0.02 M NaCl with a surface roughness of 120 grit SiC and scan rate of 30 mV/min. Figure 12 shows the results of the DL-EPR test on a solution-annealed specimen in this new condition. As seen, in this new condition, the solution-annealed specimen shows a considerable produced current at the reactivation stage. Since this specimen is solution-annealed and there is almost no sensitization, this current rises from uniform corrosion as a reuslt of the new aggressive condition. Taguchi results show that the most effective parameter in DOS measurement for both alloys is acid concentration, the lowest acid concentration among the selected concentrations. Figure 13 shows the DL-EPR results in this modified condition for solution-annealed and both sensitized specimens. Also, Table 5 represents values of DOS for the samples in the new modified condition and standard condition.

### *Analysis of Variance (ANOVA)*

Calculated values of $DF_i$, $SS_i$, $MS_i$ and ρ(%) of all factors for both specimens are presented in Table 6. As discussed above, the main factor in DOS measurement is acid concentration, which has a 42.78% and 69.83% effect for sensitized specimens at 650°C and 850°C, respectively. This shows that the acidity of the solution and, consequently, pH is the factor that highly influences the measured DOS value. In addition, as it can be seen, the influence of acid concentration in the high-sensitization condition is more significant. In other words, since in the specimen with the higher amount of sensitization, the depleted zone is wider and the passivity of this depleted zone has a higher amount of iron ion, the passivity breakdown occurs more easily in the solution with higher acidity characteristics. After the acid concentration, as it was mentioned above, the scan rate and surface roughness are significant factors influencing the DOS resolution. However, the effect of scan rate in the low-sensitization condition is much lower than surface roughness. In fact, surface roughness in the low-sensitization condition has comparable influence to that of acid concentration. However, the effect of scan rate is almost five times lower than surface roughness and almost similar to that of thiosulfate concentration. In

**TABLE 3**
*Lateral Distance Differences of the Phases to the Ditches*

| Lateral Distance Differences | Profiles in Figure 8 | | | Profiles in Figure 9 | | |
|---|---|---|---|---|---|---|
| | (1) | (2) | (3) | (1) | (2) | (3) |
| Austenite-ditch | 586 nm | 865 nm | 1.12 µm | 372 nm | 263 nm | 548 nm |
| Ferrite-ditch | 1.25 µm | 976 nm | 1.70 µm | 416 nm | 1.01 µm | 701 nm |

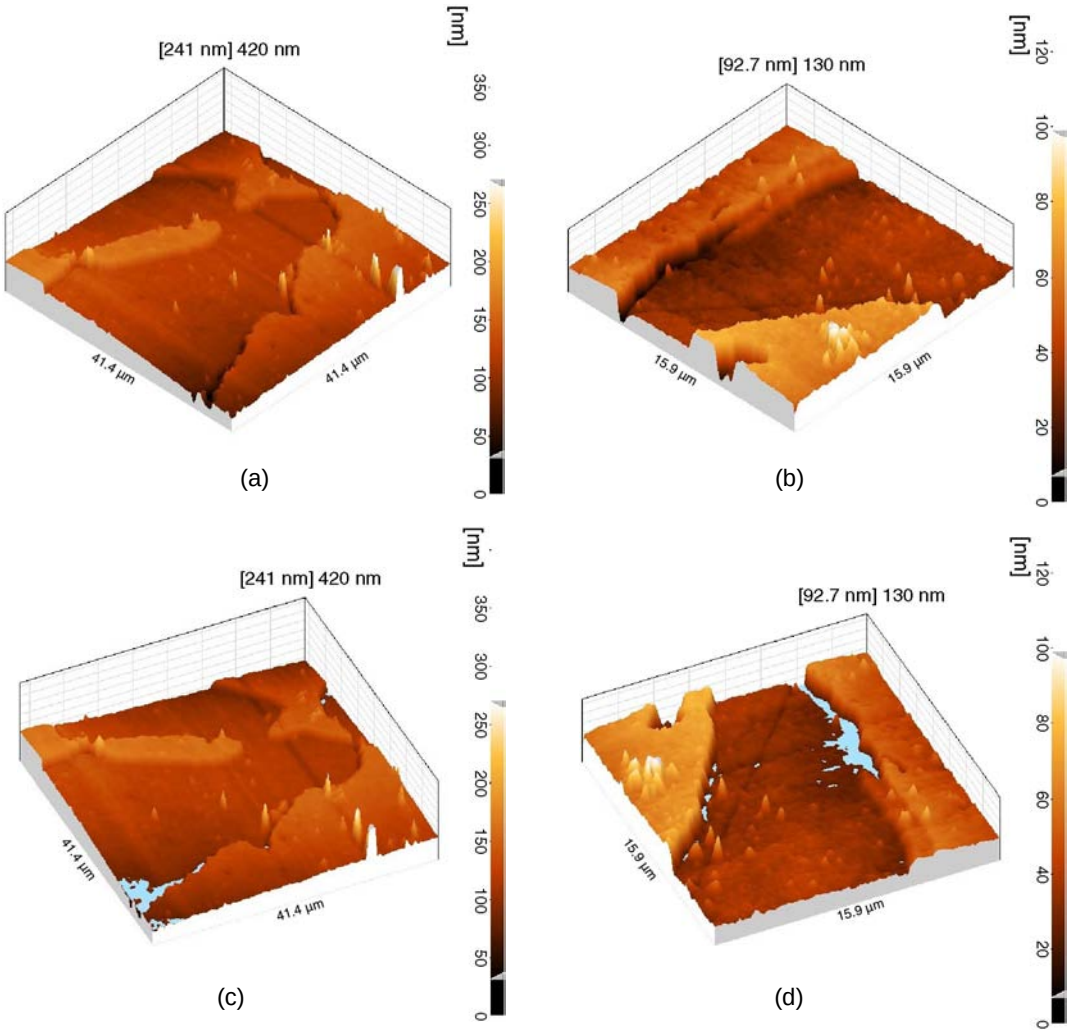


**FIGURE 10.** *Three-dimensional AFM images of 850°C sensitized sample related to the 2D AFM images in Figure 7.*

the case of the 850°C sensitized specimen, the scan rate is the most significant factor after acid concentration; however, its influence is almost 3.5 times lower than acid concentration. In this sensitization condition, the effect of surface roughness is low and comparable to that of thiosulfate concentration. For both sensitization conditions, chloride ion has the lowest effect on the DOS resolution, and its effect in 850°C sensitized sample is negligible.

## CONCLUSIONS

The DOS for DSS2205 was measured with higher resolution, by introducing a new condition based on the DL-EPR technique in $H_2SO_4$ containing two different depassivators. The results can be summarized:

- The new condition for measuring the DOS of DSS2205 is 0.5 M $H_2SO_4$, 0.005 M $Na_2S_2O_3$, 0.02 M NaCl, 120 grid surface roughness, and 30 mV/min scan rate. The new optimum condition provided higher DOS resolution and IGC detection.
- The DOS measurements in the new condition show 7.5% and 78% sensitization for the solution-annealed sample and 850°C sensitized sample, respectively, while in the previous condition, they measured 18.6% and 53.6%, respectively.
- ANOVA results showed that the effect of acid concentration on DOS measurements, for two different

**TABLE 4**

*Degree of Sensitization Value and Signal-to-Noise Ratio Calculated for Each Experiment Applied to 40 min Sensitized Specimens at 650°C and 850°C*

| Experiment No. | 650°C | | 850°C | |
|---|---|---|---|---|
| | % DOS | S/N Ratio | % DOS | S/N Ratio |
| 1 | 14.31 | 23.113 | 36.86 | 31.332 |
| 2 | 1.61 | 4.140 | 16.05 | 24.107 |
| 3 | 0.40 | –7.937 | 10.15 | 20.129 |
| 4 | 6.50 | 16.264 | 11.88 | 21.499 |
| 5 | 2.27 | 7.107 | 23.73 | 27.507 |
| 6 | 5.29 | 14.463 | 26.61 | 28.502 |
| 7 | 11.86 | 21.484 | 35.69 | 31.050 |
| 8 | 7.35 | 17.331 | 50.22 | 34.018 |
| 9 | 29.25 | 29.324 | 53.01 | 34.487 |
| 10 | 9.59 | 19.633 | 64.04 | 36.129 |
| 11 | 4.33 | 12.726 | 27.14 | 28.673 |
| 12 | 16.03 | 24.098 | 41.33 | 32.326 |
| 13 | 32.09 | 30.128 | 70.34 | 36.944 |
| 14 | 52.35 | 34.378 | 70.52 | 36.966 |
| 15 | 47.62 | 33.555 | 76.08 | 37.626 |
| 16 | 5.09 | 14.128 | 52.38 | 34.384 |

sensitization values, were not the same. It was 42.78% and 69.83% for sensitized specimens at 650°C and 850°C, respectively, while it is the most effective parameter on DOS measuring for both samples.

❖ Taguchi analysis demonstrated that for measuring the DOS of the 650°C sensitized sample, behind acid concentration, the influence of surface roughness is significant, while for the 850°C sensitized sample, after acid concentration, scan rate has the significant effect.

❖ Both ANOVA calculations and Taguchi analysis showed that, for measuring the DOS of DSS2205, the concentration of two depassivators, $Na_2S_2O_3$ and NaCl, were very low and can be negligible.

❖ Topography variations of non-sensitized and sensitized samples measured using AFM elucidated the mechanism of austenite/ferrite boundary attack and intermetallic precipitates formation in sensitized samples extended to the ferrite phase.

## ACKNOWLEDGMENTS

Authors appreciate the financial support from Ferdowsi University of Mashhad provision of laboratory facilities during the period this research was conducted.

## REFERENCES

1. A.J. Sedricks, *Corrosion of Stainless Steels*, 2nd ed. (New York, NY: John Wiley and Sons, 1996), p. 47-74.
2. K. Chandra, R. Singhal, V. Kain, V.S. Raja, *Mater. Sci. Eng. A* 527 (2010): p. 3904-3912.
3. H.D. Schulze, *VDI-Nachrichten* 47, 10 (1993): p. 28.
4. J.O. Nilsson, A. Wilson, *Mater. Sci. Technol.* 9 (1993): p. 545-554.
5. J.O. Nilsson, *Mater. Sci. Technol.* 8 (1992): p. 685-700.
6. K.L. Weng, H.R. Chen, J.R. Yang, *Mater. Sci. Eng. A* 379 (2004): p. 119-132.
7. S.S.M. Tavares, V.F. Terra, J.M. Pardal, M.P. Cindar Fonseca, *J. Mater. Sci.* 40 (2005): p. 145-154.
8. S.S.M. Tavares, V.F. Terra, *J. Mater. Sci.* 40 (2005): p. 4025-4028.

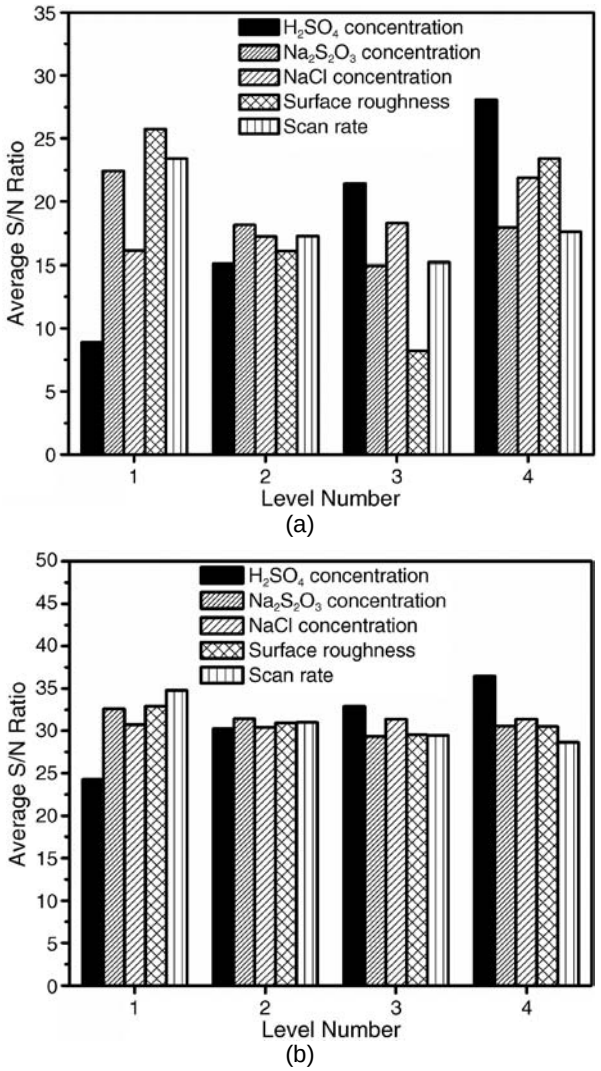


**FIGURE 11.** *Average S/N ratio for (a) 650°C and (b) 850°C sensitized samples.*

9. A. Karas, V. Cihal, V. Vanek, J. Herzan, K. Protiva, *Kovove Materialy* 25, 5 (1987): p. 497-508.
10. H.E. Buhler, L. Gerlach, O. Greven, W. Bleck, *Corros. Sci.* 45 (2003): p. 2325-2336.
11. V. Cihal, S. Lasek, M. Blahetova, E. Kalabisova, Z. Krhutova, *Chem. Biochem. Eng.* Q 21, 1 (2007): p. 47-54.
12. H. Sidhom, T. Amadou, H. Sahlaoui, C. Braham, *Metal. Mater. Trans. A* 38A (2007): p. 1269.
13. T. Amadou, C. Braham, H. Sidhom, *Metal. Mater. Trans. A* 35A (2004): p. 3499.
14. A. Kriaa, N. Hamdi, K. Jbali, H. Sidhom, *Surf. Eng. Appl. Elect.* 43 (2007): p. 494-504.
15. V. Cihal, R. Stefec, T. Shoji, Y. Watanabe, V. Kain, *Key Eng. Mater.* 261-263 (2004): p. 855-864.
16. P. Ahmadabadi, V. Kain, P.R. Singh, P.K. De, *J. Mater Eng. Perform.* 12 (2003): p. 529-536.
17. V. Cihal, A. Desestret, M. Froment, G.H. Wagner, Étude CETIM, Center de Recherches de Firminy, C.A.F.L., Rapport N, 958, 1969.
18. W.L. Clarke, V.M. Romero, J.C. Danko, *Corrosion* 77 (1977): p. 130-133.
19. M. Akashi, T. Kawamoto, F. Umemura, B. Gijutsu, *Corros. Eng.* 29 (1980): p. 163-169.
20. A.P. Majidi, M.A. Streicher, *Corrosion* 40 (1984): p. 445-458.
21. A.P. Majidi, M.A. Streicher, *Corrosion* 40 (1984): p. 584-593.
22. J.R. Scully, R.G. Kelly, *Corrosion* 42 (1986): p. 537-542.
23. S.J. Goodwin, B. Quayle, F.W. Noble, *Corrosion* 43 (1987): p. 743-747.

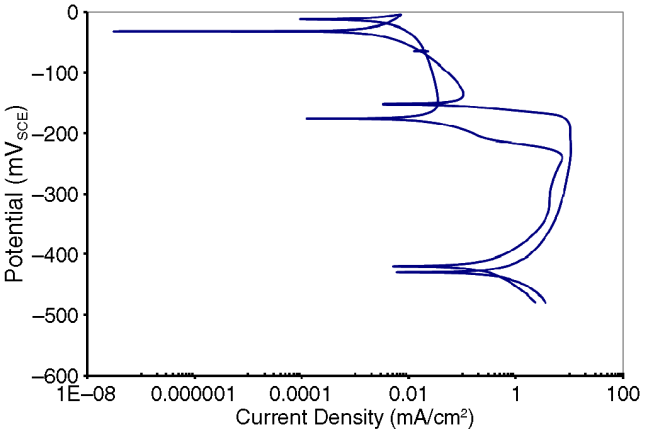


**FIGURE 12.** *DL-EPR test on solution-annealed sample in optimum new condition results from Taguchi.*

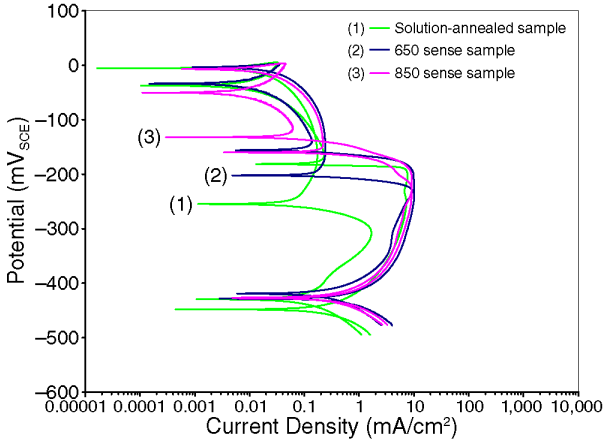


**FIGURE 13.** *DL-EPR test results in the modified condition of Taguchi solution for solution-annealed and both sensitized specimens.*

**TABLE 5**
*Degree of Sensitization Values in New Modified Condition and Previous Condition*

| Sample | Previous Condition | Modified New Condition |
|---|---|---|
| Solution-annealed | 18.6% | 7.5% |
| 650°C sensitized | 24% | 56% |
| 850°C sensitized | 53.6% | 78% |


24. D.L. Reichert, G.E. Stoner, *J. Electrochem. Soc.* 137 (1990): p. 411-413.
25. C. Liu, H. Huang, S. Chen, *Corrosion* 48 (1992): p. 686-690.
26. Z. Fang, L. Zhang, Y.S. Wu, J.Q. Li, D.B. Sun, G. Jiang, Z.M. Cui, *Corrosion* 51 (1995): p. 124-130.
27. Z. Fang, Y.S. Wu, L. Zhang, J.Q. Li, *Corrosion* 54 (1998): p. 339-346.
28. T.F. Wu, W.T. Tsai, *Corros. Sci.* 45 (2003): p. 267-280.
29. M.F. Maday, A. Mignone, M. Vittori, *Corros. Sci.* 28 (1988): p. 887-900.
30. C.D. Thual, M. Bonis, J.L. Crolet, *Mater. Corros.* 52 (2001): p. 37-44.
31. T. Amadou, C. Braham, H. Sidhom, *Metall. Mater. Trans. A* 35A (2004): p. 3499-3513.
32. C. Garcia, F. Martin, Y. Blanco, M.P. Tiedra, M.L. Aparicio, *Corros. Sci.* 51 (2009): p. 76-85.
33. M. Liljas, P. Johansson, H.P. Liu, C.O.A. Olsson, *Steel Res. Int.* 79 (2008): p. 466-473.
34. M. Momeni, M.H. Moayed, A. Davoodi, *Corros. Sci.* 52 (2010): p. 2653-2660.
35. A. Bendell, J. Disney, W.A. Pridmore, *Taguchi Methods: Applications in World Industry* (U.K.: IFS Publications, 1989).
36. G. Taguchi, *Introduction to Quality Engineering* (Tokyo, Japan: Asian Productivity Organization, 1990).
37. ASTM A262-90, "Standard Practice for Detecting the Susceptibility to Intergranular Attack in Austenitic Stainless Steels" (West Conshohocken, PA: ASTM International, 1990).
38. R.A. Kishore, R. Tiwari, A. Dvivedi, I. Singh, *Mater. Des.* 30 (2009): p. 2186-2190.
39. A. Kamyabi-Gol, S.M. Zebarjad, S.A. Sajjadi, *Colloids Surf. A* 336 (2009): p. 69-74.
40. ASTM G108-94, "Standard Test Method for Electrochemical Reactivation (EPR) for Detecting Sensitisation of AISI Type 304 and 304L Stainless Steels" (West Conshohocken, PA: ASTM International, 1994).
41. A.J. Sedriks, *Corrosion of Stainless Steels*, 2nd ed. (New York, NY: Wiley InterScience, 1996).
42. N. Ebrahimi, M. Momeni, M.H. Moayed, A. Davoodi, *Corros. Sci.* 53 (2011): p. 637-644.
43. C.H. Too, "Sensitisation of Austenitic Stainless Steels" (M.Sc Thesis, Department of Materials Science and Metallurgy, University of Camberidge, August 2002).
44. M. Momeni, A. Ale-yassin, M.H. Moayed, *Corrosion* 68 (2012): p. 015007.
45. J. Gao, Y. Jiang, B. Deng, W. Zhang, C. Zhong, J. Li, *Electrochem. Acta* 54 (2009): p. 5830-5835.
46. C.-O.A. Olsson, D. Landolt, *Electrochem. Acta* 48 (2003): p. 1093-1104.
47. I. Olefjord, L..Wecrelius, *Corros. Sci.* 31 (1990): p. 89-98.
48. S. Mischler, A. Vogel, H.J. Mathieu, D. Landolt, *Corros. Sci.* 32 (1991): p. 925-944.
49. V. Mitrovic-Scepanovic, B. Macdougall, M.J. Graham, *Corros. Sci.* 27 (1987): p. 239-247.


**TABLE 6**
*Analysis of Variance Results for All Factors Applied to Both Samples*

| Specimen | Factor | $DF_i$ | $SS_i$ | $MS_i$ | ρ% |
|---|---|---|---|---|---|
| 650°C | Acid concentration | 3 | 814.395 | 271.465 | 42.78 |
| | Thiosulfate concentration | 3 | 113.022 | 37.674 | 5.94 |
| | NaCl concentration | 3 | 74.955 | 24.985 | 3.94 |
| | Surface roughness | 3 | 752.220 | 250.740 | 39.51 |
| | Scan rate | 3 | 149.142 | 49.714 | 7.83 |
| 850°C | Acid concentration | 3 | 318.098 | 106.033 | 69.83 |
| | Thiosulfate concentration | 3 | 21.964 | 7.321 | 4.82 |
| | NaCl concentration | 3 | 3.080 | 1.027 | 0.68 |
| | Surface roughness | 3 | 24.181 | 8.060 | 5.31 |
| | Scan rate | 3 | 88.208 | 29.403 | 19.36 |